Published in: **Process Safety and Environmental Protection, 89, p371-381, 2011**

Factors affecting vapour production in large scale evaporating liquid cascades

S. Coldrick[1a], S. E. Gant[a], G.T. Atkinson[a], R. Dakin[b]

[a]Health & Safety Laboratory, Harpur Hill, Buxton, SK17 9JN, UK.

Tel: +44 (0)1298 218239; Fax: +44 (0)1298 218840

E-mail address: simon.coldrick@hsl.gov.uk

[b]Health and Safety Executive, Redgrave Court, Merton Road, Bootle, L20 7HS.

Research highlights

- A CFD model for predicting vapour production from flammable liquid cascades is developed.
- The model is validated against a unique series of large scale experiments.
- Different cascade configurations beyond the experimental range are investigated.

Keywords

Tank overfilling, cascade, CFD, source model, Buncefield.

Abstract

This paper presents a Computational Fluid Dynamics (CFD) model of the evaporating liquid cascade produced in a large hydrocarbon storage tank overfilling incident. The model is first validated against the results of a unique series of full-scale experiments,

[1] Corresponding author

in which liquid hexane was released from a 10 metre high tower. Comparisons are presented for the temperature of both the liquid and vapour in the cascade, and the temperature of the vapour current. The validated model is then used to investigate the effects of different tank bund configurations, and the influence of an accumulating vapour layer on the vapour production process.

1 Introduction

Evaporating liquid cascades resulting from tank overfilling incidents have proved to be an effective means of creating a flammable vapour cloud. Both the recent tank overfilling incidents at Buncefield (MIIB, 2006) and at the Caribbean Petroleum Corporation fuel depot in Puerto Rico on 23 October 2009 produced very large vapour clouds which ignited and led to extensive damage. In the cascade, falling liquid is mixed with a continuous supply of fresh air and the droplets provide a large surface area for evaporation. The resulting vapour is forced out at the base of the cascade, producing a dense, initially fast-moving, current that disperses across the ground and mixes with the surrounding air.

To investigate the formation of a vapour current from an overfilling tank, a series of experiments and Computational Fluid Dynamics (CFD) simulations have recently been carried out at the Health and Safety Laboratory (HSL). Early results from this work were reported by Coldrick et al. (2011). The present paper reports the findings of a more recent second series of experiments and simulations, building on the previous experience. Additional instrumentation has enabled more detailed measurements to be made of temperatures within the cascade. A more sophisticated

CFD model has also been constructed and validated using the experimental data. This new model has been used to identify the key cascade parameters that control the vapour production mechanism. The effects of various different bund configurations have also been investigated.

2 Cascade experiments

The experimental apparatus, shown in Figure 1, consisted of a small liquid storage tank set on top of a 10 m high tower. Pressurised air was used to drive the liquid out of the storage tank and down the spill chute where it was projected outward. A deflector plate (deflector plates are fitted to tanks for use in fire situations to deflect water pumped onto the roof of the tank onto the sidewalls, see Gant and Atkinson, 2007) was not fitted to the end of the chute, so that all the liquid was directed into a single free cascade. Measurements were made of the liquid temperature in the spill chute and of the ambient temperature at several reference locations near the tank. Simultaneous independent measurements were made of the liquid and vapour temperatures at the base of the cascade. The liquid temperatures were measured using an array of collecting pots each equipped with a thermocouple at their base. Vapour temperatures within the cascade were measured by an array of aspirated thermocouples. These were essentially inverted versions of the liquid collecting pots connected by small diameter tubing to a vacuum pump. The pumping rate was sufficiently large to draw vapour from the cascade upward past the thermocouple whilst excluding droplets. In addition to the cascade measurements, an array of thermocouples was positioned downstream of the cascade to record the temperature of the vapour current.

3 Computational model

In the present work, the general-purpose CFD software, CFX 12.1 was used to model the release tower, liquid cascade and vapour current. The approach taken was similar to that used previously in the preliminary investigation by Gant and Atkinson (2007) and Coldrick et al. (2011). The flow of air and vapour was modelled using an Eulerian model, which involved a computational mesh that was fixed in space through which the gases flowed. Momentum, mass and energy conservation equations were solved in each mesh cell to find the velocity, temperature, pressure and concentration distributions. The spray of droplets was modelled using a Lagrangian approach in which the paths of discrete computational particles were tracked through the flow domain from their injection point until they hit a solid surface, escaped the domain or evaporated completely.

The exchange of momentum, mass and heat between the Eulerian phase and Lagrangian particles was two-way. For momentum, particles falling through the air were subjected to drag forces, and their trajectories were affected by turbulent perturbations in the air. The air was also affected by the drag of the droplets and was entrained into the spray. Two-way coupling was important in determining evaporation rates, where the vapour concentration in the gas phase affected the rate of evaporation from the droplets and vice versa. Droplet evaporation led to a temperature decrease which affected the saturation vapour pressure and hence the calculated evaporation

rate. Coupling between the two phases was achieved by introducing source terms derived from the Lagrangian solution into the Eulerian transport equations. The overall CFD solution was obtained by iterating between the Eulerian and Lagrangian models.

In previous simulations reported by Coldrick et al (2011), the cascade of liquid was modelled as a collection of particles injected from slots on the front face of the release tower. The current study aimed to examine the effect of various cascade parameters more closely and therefore a different approach was taken to release the spray droplets. The release tower was approximated as a rectangular box located on a flat surface as shown in Figure 2. The flow domain included a 30 × 30 × 20 m section of atmosphere to account for expected air movements. A projection, rather like a short diving board, was positioned at the top of the release tower. Particles were then injected downwards from a horizontal rectangular area in space at the end of the diving board using a custom droplet-injection routine. This arrangement allowed for variation of the width and depth of the cascade and its offset from the release tower. Particles were injected uniformly at randomly assigned locations within the specified area at each injection cycle.

An unstructured computational mesh was used with cells more densely clustered near the release points, along the trajectory of the spray particles and close to the floor. Near the liquid cascade, cell sides were typically a few centimetres across, whilst in the far field they were around one metre or more. Tetrahedral cells were used in the majority of the flow domain, whilst prism-shaped cells were used near the ground to

increase the number of cells in the vertical direction and resolve the thin, dense, gravity current.

The open boundaries at the domain sides and top (representing the atmosphere) were set as entrainment boundaries, allowing the air velocities to freely develop whilst maintaining a set hydrostatic pressure. The 20 m domain height means that hydrostatic pressure has a significant effect on the density. Rather than specifying a uniform constant pressure, an analytical profile was used.

Turbulence was modelled using the industry standard SST model (Menter, 1994). At the start of the simulations, when the liquid first begins to cascade from the tank, it was assumed that the air velocity was zero everywhere (i.e. the air was quiescent). A very low but finite initial turbulence level was also specified: an initial turbulence intensity of 5% (based on a reference velocity of 0.01m/s) and a ratio of the turbulent viscosity to the fluid viscosity of 10. A non-Boussinesq approach was adopted to model buoyancy effects, which is suitable for modelling a wide range of density variations. The effect of density variations on the flow turbulence was accounted for using standard buoyancy corrections in the turbulence transport equations, for details see ANSYS (2009).

Gant and Atkinson (2007) noted previously that splashing droplets at the base of the cascade may be of importance in altering the vapour current properties. Splashing has the effect of reintroducing droplets at the base of the cascade. The splashing models available in CFX are tailored to applications such as internal combustion engine fuel injection and limited success was found in using them for the current application. Instead, the effects of splashing were accounted for by a secondary injection of

particles at the base of the cascade, with a prescribed size, mass flow, temperature and velocity. The particles were injected upwards from the ground in a cone pattern with a base diameter of 1.5 m. The splashing droplets were injected in such a way as to match the behaviour observed in the experiments.

During the course of the transient CFD simulations, several outputs from the model were monitored: the total vapour volume, cascade vapour temperature and vapour current temperature. The total vapour volume was calculated as the volume integral of vapour in the domain added to the time integral of the vapour leaving the domain through the open boundaries. Vapour temperatures were monitored at locations corresponding to the measurement locations. Cascade liquid temperatures were also obtained at the end of the simulation period by post-processing the droplet temperature, which were stored as part of the particle-tracking information. The equivalent liquid pot temperatures were obtained by exporting the location, temperature and mass of each particle for the entire period of the release. The data were then filtered to determine those particles whose positions corresponded to the position of each liquid pot. The temperatures of all the particles in each pot were then mass-averaged to give the liquid pot temperatures for the steady state period of the release. Additionally, a mass-averaged liquid temperature for all droplets for the entire simulation was obtained for all of the droplets at a location just above the ground, at the base of the cascade.

3.1 Sensitivity analysis

A sensitivity analysis was undertaken to examine the effect of various numerical model input parameters on the resulting flow predictions. These input parameters included: the mesh size, computational time-step, number of iterations per time-step, particle injection speed and number of particles. It was necessary to set a particle injection speed in the model in order to introduce new spray droplets into the flow domain. A low velocity was used for this since, in reality, a tank overfilling release does not impart a significant initial downward momentum to the liquid, which is instead primarily gravity driven.

A full factorial sensitivity study of these five input parameters would have required at least 2^5 =32 simulations. Whilst this type of approach has been used for CFD simulations previously by Cervantes and Engström (2004), it was not feasible for the present application, since a single simulation typically required around one day to compute. To reduce the total number of simulations required and maximise the information gained, an experimental design technique was used, similar to that tested by Hicks and Turner (1999) and Sacks et al (1989). Each of the inputs was set at two levels and a fractional factorial design (see Hicks and Turner 1999) was used to reduce the number of simulations required to 8. Table 1 lists the high and low values of each variable and Table 2 gives the settings used for the 8 runs. Other computational inputs are listed in Table 3. The output variables examined in these tests were the total vapour volume, the average liquid temperature and the average vapour temperature at the base of the cascade.

Results of the fractional factorial sensitivity analysis are shown in Figure 3. The effect of each input variable was calculated from the difference between the high and low

values for each input parameter, as a percentage of the mean over all eight simulations. The largest effect was clearly the mesh size, which accounted for roughly 20% of the total variation. As a result of this, an independent test of mesh sensitivity was carried out to determine a suitable mesh size for the simulations. The other inputs tended to have small effects on the three output variables.

3.2 Exploratory simulations and validation

A number of physical input parameters to the CFD model were the subject of significant uncertainty. For a given release rate of liquid from an overfilling tank, it is difficult to establish from theoretical considerations alone the trajectory of the droplets and initial spreading rate of the spray. The precise details of the resulting flow behaviour are a complex function of the tank top design (or spill chute) and the primary breakup mechanism, from a continuous liquid stream into fluid ligaments and spray droplets. Similarly, the nature of splashing at the base of the cascade is complex and the proportion of re-suspended liquid, its trajectory and size spectrum, cannot easily be quantified without recourse to detailed experiments.

To address these issues, exploratory simulations were performed to adjust the CFD model to fit one of the experimental datasets. These simulations concentrated on the physical (as opposed to the numerical) aspects of the model, and included tuning parameters such as the cascade inlet dimensions, droplet size distribution and splashing conditions (further details are provided in the next section). The model parameters were systematically varied within reasonable ranges until a good fit with the data was obtained. In the first step, the cascade dimensions in the CFD model

were specified to match the behaviour observed in the experiments. Then the initial size spectrum of the droplets was specified, using a Rosin-Rammler distribution. This size distribution is specified by two parameters: a characteristic diameter (δ) and an index that controls the spread in droplet sizes (γ). It was found that the average liquid temperature in the cascade was primarily controlled by δ, but was relatively insensitive to changes in γ. Therefore, simulations first concentrated on finding the value of δ which gave the correct average liquid temperatures. Then γ was adjusted to match the vapour temperatures in the cascade. Once the liquid and vapour temperatures in the cascade were predicted well by the CFD model, the splashing conditions were adjusted in order to obtain good agreement with the measured temperatures of the vapour current.

Two separate experiments were used for these comparisons, which had different release rates and ambient conditions. The model was first adjusted to fit the test 9 data, denoted "Case A" and then used independently (without further adjustment) to predict the flow behaviour in test 12, denoted "Case B". The modelled conditions are given in Table 4.

The predicted mass-averaged liquid temperatures for Case A across the depth of the cascade are shown in Figure 4. These were obtained for the period between 10 and 60 seconds after the start of the release, when the flow had reached a steady state. The solid line represents the mass average temperatures and error bars indicate the maximum and minimum droplet temperatures obtained at each location. The mean liquid temperatures (number weighted, rather than mass-averaged) are also shown with a dotted line. A single value from the experiments is plotted as the horizontal

dashed line. This corresponds to the average temperature from a single liquid pot which was reliably being impacted by the cascade and therefore corresponds to the mass average liquid temperature at the cascade centre. Due to the ratio of surface area to volume, large droplets tend to stay relatively warm, whereas small droplets can reach very low temperatures. At the edges of the cascade, the vapour concentrations are low and hence droplets can readily evaporate. In the core of the cascade, the vapour concentrations are higher, evaporation is more limited and hence droplet temperatures tend to be higher. Therefore, at the edges of the cascade, relatively few droplets were collected and these tended to be very small and cold.

The bulk liquid temperature given by the large mass of liquid at the centre of the cascade in Figure 4 provides an indication of the overall degree of evaporation. However, a small proportion of the injected mass was contained in very fine droplets. Although these fine droplets contributed to the total vapour production, some of their effect was not registered in Figure 4, since a proportion of these droplets were either carried away or evaporated completely before they could arrive at the measuring point. The liquid temperatures should therefore not be relied upon solely to determine the total amount of evaporation. Figure 4 also highlights the difficulty faced in assessing the degree of saturation of the vapour in the cascade. Small, cold droplets may not be able to evaporate whilst larger, warm droplets can still evaporate, although their contribution will be limited, due to their smaller ratio of surface area to volume.

The predicted and measured minimum vapour temperatures within the cascade are shown in Figure 5. In the first 20 seconds of the release, the profiles exhibit different behaviour, with the CFD model showing an immediate temperature drop followed by

a recovery to a steady state whereas in the measurements there was a more gradual decline to the steady state. The sudden initial temperature drop in the CFD model results was caused by the droplets falling initially through fresh air. In this short period, significant evaporation took place and therefore the predicted temperatures were low. The gradual decrease in the measured temperatures is considered to result from a time delay related to the thermal mass of aspirated thermocouples and flow recirculation effects within the devices. The gradual reduction in temperatures also appeared to be linked to a recirculation of cold vapour in the region behind the cascade. This effect took up to 20 seconds to become established fully. Tests with the CFD model suggested that the significance of the flow recirculation effects was dependent on the proportion of fine droplets present. In the experiments, it was likely that the droplet size spectrum changed over time. Very fine droplets were probably produced initially, when the relative velocity between the falling droplets and the quiescent ambient air was greatest. The recirculation of these fine droplets within the region between the cascade and the tank wall, may have then led to the gradually declining vapour temperature in the cascade. Such subtle effects cannot easily be accounted for in the CFD model, which uses a fixed droplet size spectrum that was tuned to obtain the correct steady-state temperatures.

The predicted and measured vapour temperatures at a position 0.5 m from the ground and 5 m from the release tower are shown in Figure 6. The arrival of the cold vapour current is clearly evident in the experimental trace and visible as a slight dip in the CFD profile. The CFD temperatures then undergo a rapid cooling after around 10 seconds. The reason for the lag in the predicted temperature drop is not clear but is likely to be due to assumptions made in the prescription of the splashing droplets in

the model. Despite these differences, the predicted steady-state temperature is within one degree of the measured value. The temperature profiles at the 5 m mast were used as a benchmark to adjust the splashing droplet size and mass flow (see also Section 3.5).

3.3 Identification of important parameters

The exploratory process of fitting the CFD model to the experimental data resulted in an increased understanding of the vapour generation processes. Coupled with this, the previous systematic variation of model input parameters resulted in a large results dataset. This dataset was used to examine the relative importance of several input parameters as follows:

Droplet size – Simulations were performed with both a mono-sized droplet spectrum and a Rosin-Rammler size distribution, in which a representative diameter and spread were specified.

Number of particles – Whilst the number of particles was investigated previously (see Section 3.2), this factor was revisited once the particle size distribution that best fitted the measurement data was found. It is a potentially important parameter, since a particle size distribution usually requires the simulation of a greater number of particles than if a mono-sized droplet spectrum is used. The sensitivity of the results

to the number of computational particles was assessed both for those injected in the cascade and those in the splash zone.

Turbulent dispersion – As droplets pass through the air, their trajectory may be affected by turbulent perturbations or localized eddy motion. This was accounted for in the CFD model by using the particle turbulent dispersion model of Gosman and Ioannides (1981). Tests were performed without this model to examine the sensitivity of the results to the effect of turbulent dispersion.

Wall heat transfer – The vaporisation rate could potentially be influenced by heat transfer from the ground and the release tower walls. Simulations were performed with different thermal boundary conditions on these surfaces to assess the degree of sensitivity in the model predictions. Tests were performed using constant temperature walls, adiabatic walls or a model that accounted for heat transfer through the concrete floor at the base of the cascade.

Droplet breakup – Simulations were performed using the droplet breakup model of Rietz and Diwakar (1986) in conjunction with an initial droplet size distribution. The model accounted for aerodynamic breakup of particles as a function of the particle speed relative to the surrounding gas phase.

Cascade dimensions – The cascade dimensions were initially specified in the CFD model using photographs taken during the experiments. In addition to this, simulations were carried out using a range of cascade heights, widths, depths and offsets from the release tower wall.

Splashing droplet size and mass flow – Splashing droplets at the base of the cascade were represented by a separate vertical injection of spray particles with an initial temperature equal to the average temperature of cascade particles striking the ground. The influence of splashing droplets was assessed by varying their initial size and mass flow.

For these sensitivity tests, the model outputs used for the comparison were again the cascade liquid and vapour temperatures and the total amount of vapour produced over the simulation period. Due to the large number of variable parameters, a full parametric study was not undertaken and the dataset did not include a full breakdown of the effects of varying one parameter at a time. Results were therefore examined using the coefficient of variation (CV), defined as the ratio of the standard deviation (σ) to the mean (μ):

$$CV = \frac{\sigma}{\mu} \tag{1}$$

The coefficient of variation is a means for comparison of the *relative* effects of each of the inputs on each of the outputs. Figure 7 shows the coefficient of variation for the three output parameters for a number of input parameters. The total vapour volume was almost equally affected by the cascade droplet size, the splashing droplet size and mass flow, but the largest influence was from the cascade dimensions. Including a model for turbulent dispersion had the effect of increasing the spray width, and therefore had a significant effect on the total vapour volume. The wall heat transfer treatment had a relatively small effect, indicating that the production of vapour was

governed by mixing with ambient air, rather than heat transfer from neighbouring solid surfaces. The overall vaporisation rate was largely uninfluenced by the numbers of particles.

The cascade liquid and vapour temperatures were mainly a function of the droplet size within the cascade, and the cascade dimensions. This was expected, since the temperatures were linked directly to the effectiveness of mixing between air and liquid within the cascade. Spreading the particles over a larger area increased the available air for mass transfer, and similarly, decreasing the particle size resulted in a greater surface area for mass transfer. The liquid temperature appeared to be affected by the number of particles in the cascade. This was a symptom of the method of assessing the liquid temperature: more particles resulted in an increased likelihood of collecting particles in the liquid pots in the model, and an improved statistical measure of the mean liquid temperature. The vapour temperature was insensitive to the number of droplets in the cascade, but sensitive to the number of splashing particles. This is likely to have been due to very small splashing particles being caught in the flow recirculation behind the cascade and then re-entrained into the cascade flow. The more particles that were injected, the greater this effect had on the results. The model results shown subsequently used the maximum number of droplets that were practical, given the computing resources available.

3.4 Effect of splashing droplets

The effect of splashing droplets is readily illustrated by examining the vapour current properties with distance from the tower wall. Figure 8 shows the vapour current

temperature and concentration on a line extending 10 m perpendicular to the release tower wall, at 0.15 m height from the ground. The values shown were extracted towards the end of a simulation once a steady state had been reached. Three simulations are presented: 1.) without splashing, 2.) splashing with a fixed post-impingement droplet diameter of 0.1 mm monosize droplets, and 3.) splashing with a post-impingement droplet size spectrum specified using a Rosin-Rammler distribution with $\delta = 1$ mm and $\gamma = 1.5$. Splashing mass flow rates for simulations 2 and 3 were 10% and 50% of total liquid flow released from the tank, respectively. The peak concentration and lowest temperature shown for the non-splashing case correspond to the location of the center of the cascade. Concentrations and temperatures show opposite trends, since dilution and temperature rise are interlinked and there is very little additional vaporization outside of the cascade for the non-splashing case. For both cases with splashing droplets, the vapour temperature surrounding the cascade is approximately equal to the splashing droplet temperature. A slightly higher initial concentration is obtained for Case 3 in the region of the cascade. This is likely to be due to the presence of some very fine droplets that evaporate readily. Outside of the splashing zone, there is an immediate increase in temperature for this case. For Case 2, the monosize 0.1 mm droplets produce some further evaporation outside of the splash zone, and hence a further temperature drop, before the vapour current begins to warm by entrainment of fresh air. This appears to be due to a greater proportion of the droplets being carried downstream by the vapour current for this case. It is interesting to note that the two splashing droplet sizes and mass flows used ultimately result in the same concentration being produced. The different prescriptions of splashing droplets were found to result in similar velocity fields along the vapour current. For the effect of splashing relevant to this problem, the fluid

mechanics and thermodynamics of the vapour current are effectively uncoupled. Similar velocity fields imply similar levels of mechanical mixing independently of the temperature and concentration fields.

Many more splashing simulations have been performed than are presented here, which showed that the concentrations and temperatures in the vapour current are sensitive to both the proportion of released liquid mass flow rate that is splashed back into the air, and the size spectrum of the splashed droplets. Further investigation is required to fully understand these effects and to develop a generic splashing model. Previous work on this subject, in the context of internal combustion engines, was reported by Bai et al. (2002). They showed that splashing on a wetted wall could potentially result in the reintroduction of 110% of the liquid mass flow rate, and hence substantially increased vapour production. Comparison of simulations with and without splashing droplets showed that typically 20-30% greater vapour volume was achieved with a splashing mass flow of 10% of that in the cascade.

3.5 Model summary

A CFD model has been developed of a liquid cascade in conjunction with a series of experiments. Various input variables have been identified and used to adapt the model to give good agreement with the experimental data. Several conclusions can be drawn from analysis of the outputs from the model:

Establishment of a vapour current is a transient process. From the initial impact of droplets with the ground, there is a time period over which a recirculation of vapour

into the cascade is established. This recirculation results in a gradual cooling of the vapour current. Steady-state conditions are usually established after around 20 seconds.

Liquid and vapour temperatures within the cascade depend greatly on the droplet size and size distribution within the cascade. Small droplets evaporate readily (and possibly completely) and produce low vapour temperatures, whilst liquid temperatures are primarily dictated by the remaining large droplets. Liquid and vapour temperatures are therefore not coupled directly.

Splashing droplets govern the vapour current properties almost independently of conditions in the cascade. The effect of splashing droplets is to contribute to the concentration and total vapour volume whilst reducing the temperature in the vapour current. The temperature and concentration in the current depends on the size spectrum and mass flow rate of the splashing droplets.

4 Further use of the model

The previous sections have presented CFD simulations of tank overfilling releases and have examined the model sensitivity to its input parameters. Two cases have been developed which show good agreement with the vapour and liquid temperatures measured in full-scale experiments (Table 4). In this section, a further set of simulations are described in which the validated model is used to examine the effects of various bund configurations on the vapour concentrations. The effect of multiple adjacent release points – as encountered on a circular tank (see Gant and Atkinson,

2007) – is also considered. Figure 9 shows the geometry used for these simulations, consisting of a 20 m diameter circular tank located centrally within a bunded area, with eight release points equi-spaced around the tank roof. Computing requirements for the simulations were reduced by taking advantage of symmetry, and only one quarter of the flow domain was modelled. The section of the geometry used for the model is indicated by the wireframe in Figure 9. Two injection locations were specified, with the injection parameters corresponding to those used previously for Case B (see Table 4). Two simulations were performed without a bund, and four simulations were performed with different bund configurations, as listed in Table 5. In the first simulation without a bund (Case C), an unobstructed ground plane was modelled and the vapour was allowed to escape the flow domain unimpeded. In the second simulation without a bund (Case H), a 4 m high wall was placed at the edges of the flow domain to simulate the effect of a gradually accumulating vapour layer.

A number of outputs were monitored over the course of the simulation period. These included the average vapour concentration within the bund, the concentration of material flowing over the top of the bund and the concentration of vapour just outside the bund. Simulations were continued until the average vapour concentration within the bund reached a steady state.

4.1 Liquid and vapour temperatures in the cascade

Figure 10 shows the liquid temperature profiles for the six cases given in Table 5, presented alongside the results for the single release Case B. The liquid temperature profiles are taken as the average over the steady-state period of the release, from 10-

60 seconds. It can be seen that the different bund configurations have minimal effect on the liquid temperature profiles. The cascade vapour temperatures (Figure 11) show that the presence of adjacent release points leads to a small reduction in vapour temperature within the cascade, generally less than one degree, as compared to the case with the single release (Case B). This may be in part due to additional cold vapour being available at the sides of the cascades. As vapour begins to accumulate within the bund, an increasing amount of cold material is recirculated back into the cascade. This manifests itself as a slight reduction in the liquid and vapour temperatures in the cascade. Table 6 shows the differences in the averaged liquid and vapour cascade temperatures between the first 60 seconds and the last 60 seconds of each simulation. Both liquid and vapour temperatures undergo a small reduction, as a result of the recirculation.

4.2 Concentration and temperature in the bund

For the simulations with bunds (Cases D, E, F and G), the average concentration within the bund was defined as the volume integral of concentration for all cells within the bund (below the bund height), divided by the total volume of the bund. The average temperature was similarly defined. In all of the cases modelled, the bund height was 2 m. Figure 12 shows the development of the average concentration and temperature over time for the four cases. Cases E, F and G all eventually lead to similar steady state concentrations of around 0.025 mol/mol, despite the bund wall being spaced at different distances from the tank, or for the bund to have a sloping rather than a vertical wall. However, Case D leads to a slightly higher steady state average concentration of 0.028 mol/mol. The bund wall was located closest to the

tank for this case, and the higher concentration resulted from the vapour current inside the bund having little opportunity for dilution. For all cases, the behaviour observed in the average concentration is mirrored in the temperature profiles, all exhibiting a drop of approximately 6 °C. The relationship between the average concentration within the bund and that of the material flowing over the top of the bund wall is illustrated in Figure 13 for Case E (bund at 10 m). At a point on top of the bund wall directly opposite the cascade, the peak concentration is slightly higher than the average as this is where the body of the vapour current passes over the bund wall. On top of the bund wall in between the two cascades, the vapour concentration matches the average inside the bund. This behaviour was observed for all of the bunded spills, indicating that the steady state mean concentration within the bund is a good approximation for the vapour source term arising from a spill into a bund.

The shape of the vapour clouds produced by the different bund configurations are shown in terms of isosurfaces at the Lower Flammability Limit (LFL) concentration for hexane of 0.012 mol/mol in Figure 14. The isosurfaces are coloured with height from the ground up to a maximum of 2 m, (corresponding to the bund height). The images are mirrored in the symmetry planes and a section of the isosurface has been removed to show the bund geometry. In each case, rapid entrainment into the vapour current close to the cascade impact point draws fresh air down into the vapour layer, causing a deformation of the isosurface. For Case D, and to a lesser extent Case E, the high-momentum stream of vapour produced by the cascade leads to a deformed surface of the vapour layer even outside the bund, whereas in Cases F and G it is more uniform.

4.3 Effect of accumulating vapour layer

In an overfilling incident, vapour is not necessarily free to travel away from the immediate vicinity of the tank. Topographical features and obstacles may result in an increasingly deep layer accumulating and surrounding the tank. This was observed in the Buncefield incident where the CCTV records showed a mist increasing in depth over a 23 minute period to around 4 metres in the area adjacent to the bund in which the tank was overfilling (Gant and Atkinson, 2011). Simulations reported by Coldrick et al. (2011) examined the effect of an accumulating vapour layer on the concentration of material overflowing from the bund. This effect was examined further in the current study using the Case H arrangement (see Table 5), in which there was no bund but a 4 m high wall was placed at the flow domain boundaries. During the course of the simulation, the average vapour concentration within the 4 m tray and the depth of the layer corresponding to ½ LFL (a concentration of 0.006 mol/mol) were monitored. The former quantity was calculated from the integral of all computational cell volumes with concentration over ½ LFL, divided by the total area of the ground. The simulation was continued until the concentration reached a steady state. This required approximately 15 minutes simulation time, corresponding to 17 days computer run time using a four-processor workstation.

Figure 15 shows that the vapour depth is relatively quickly established, taking 200 s to reach a depth of just over 4 m. At this point, vapour begins to spill over the outer wall. The average concentration within the 4 m tray increases steadily over time, levelling out after around 13 minutes. The recirculation process reaches a steady state, giving a final concentration of 0.035 mol/mol or approximately three times the LFL.

The increased concentration obtained in comparison to the bunded spills is caused by the increased layer depth of 4 m as opposed to 2 m. An increased layer depth results in a larger proportion of vapour being recirculated into the cascade and hence a higher concentration. However, the maximum concentration is always limited by the entrainment of fresh air that is pulled downwards into the vapour cloud by the cascade. This is illustrated in Figure 16 showing an isosurface at twice the LFL, coloured according to the height from the ground. Twice LFL has been used for illustration purposes of the higher average concentration achieved in this case. In the region immediately surrounding each cascade, the vapour layer is clearly displaced by the motion of the entrained ambient air.

5 Conclusions

CFD models of evaporating liquid cascades have been developed and validated using data from a series of large-scale experiments. Predictions from the CFD models have been compared to measurements of the liquid and vapour temperatures at the base of the cascade and the temperature of the vapour current moving away from the base of the cascade.

Sensitivity studies have shown that the total amount of vapour produced by the liquid cascade is strongly influenced by the cascade dimensions, the droplet size distribution and the presence of splashing at the base of the cascade. The liquid and vapour temperatures in the cascade itself were found to be primarily affected by the cascade dimensions and droplet size distribution, and were unaffected by splashing. Heat transfer from surrounding solid surfaces was found not to influence the results

significantly, i.e. vaporisation was largely driven by mixing and evaporation of the liquid droplets into the entrained ambient air. The presence of splashing droplets was found to contribute significantly to the overall vapour production. Splashing droplets are effectively a means of vaporising additional liquid into the current leaving the cascade.

In addition to the properties of the isolated vapour cascade, it is of practical interest to examine the effects of tank bunds on the generation of vapour by the cascade. A series of simulations were carried out using a circular tank geometry with a number of different bund configurations. In each case it was found that vapour would gradually accumulate within the bund with increasing concentration until a steady state was achieved. In the steady state, ambient air drawn downwards into the vapour layer by the cascade would ultimately act to limit the maximum concentration to approximately two-thirds of that obtained at the base of the cascade for a 2 m high bund. The different bund configurations studied were all the same depth and therefore very similar average concentrations within the bunds were achieved.

The effect of a gradually deepening vapour layer, more than 4 m thick, was shown to increase the re-entrainment of vapour into the cascade. Higher vapour concentrations were produced of the order of four-fifths that obtained at the base of the cascade. However, the fresh air was still drawn into the upper portion of the cascade, which limited the maximum concentration produced in the vapour layer.

The present work has considered cascade releases of a pure substance, liquid hexane. Future work will examine releases of a multi-component mixture, such as petrol. The

behaviour of droplets may be different for this case, since the heavier fractions present in petrol are likely to evaporate very slowly, if at all, unlike pure hexane where the very fine droplets evaporated completely. Whether this will lead to significant differences in terms of the overall volume of vapour produced remains to be seen. The final goal for this research will be a source model for tank overfilling releases that can be used as an input to an appropriate gas dispersion model.

Acknowledgements

This publication and the work it describes were funded by the Health and Safety Executive (HSE). Its contents, including any opinions and/or conclusions expressed, are those of the authors alone and do not necessarily reflect HSE policy.

References

ANSYS (2009) ANSYS CFX-12.1 User Guide. ANSYS, Inc., Canonsburg, Pennsylvania, USA.

Bai, C.X., Rusche, H., Gosman, A.D., 2002. Modeling of gasoline spray impingement. Atomization and Sprays 12, 1-27.

Cervantes, M.J., Engström T.F., 2004. Factorial design applied to CFD. J. Fluids Eng. 126, 791-798.

Coldrick, S., Atkinson, G.T., Gant, S.E., 2011. Large scale evaporating liquid cascades - an experimental and computational study, Proc. IChemE Hazards XXII Symposium, Liverpool, UK, Rugby: IChemE. In press.

Gant, S.E., Atkinson, G.T., 2007. Flammable vapour cloud risks from tank overfilling incidents. Health & Safety Laboratory Report MSU/2007/03 (Available from the Health and Safety Laboratory).

Gant, S.E., Atkinson, G.T., 2011. Dispersion of the vapour cloud in the Buncefield Incident. Process Safety and Environmental Protection, NOTE FOR PSEP EDITOR, THIS PAPER HAS ALSO BEEN SUBMITTED FOR THE HSL CENTENARY SPECIAL EDITION.

Gosman, A.D., E. Ioannides, 1981. Aspects of computer simulation of liquid fuelled combustors. AIAA Paper 81-0323.

Hicks, C.R. and Turner Jr, K.V., 1999. Fundamental concepts in the design of experiments. Fifth edition, Oxford University Press.

Menter, F.R., 1994. Two-equation eddy-viscosity turbulence models for engineering applications. AIAA J. 32, 1598-1605.

MIIB, 2006. Buncefield Investigation Progress Report, (available from http://www.buncefieldinvestigation.gov.uk, accessed November 2010). Major Incident Investigation Board (MIIB).

Reitz, R.D. and Diwakar, R., 1986. Effect of drop breakup on fuel sprays. Society of Automotive Engineers Technical Paper 860469, SAE Transactions , Vol. 95, Sect. 3, pp. 218-227

Sacks, J., Schiller, S.B. and Welch, W.J., 1989. Designs for computer experiments. Technometrics 31, 41-47.

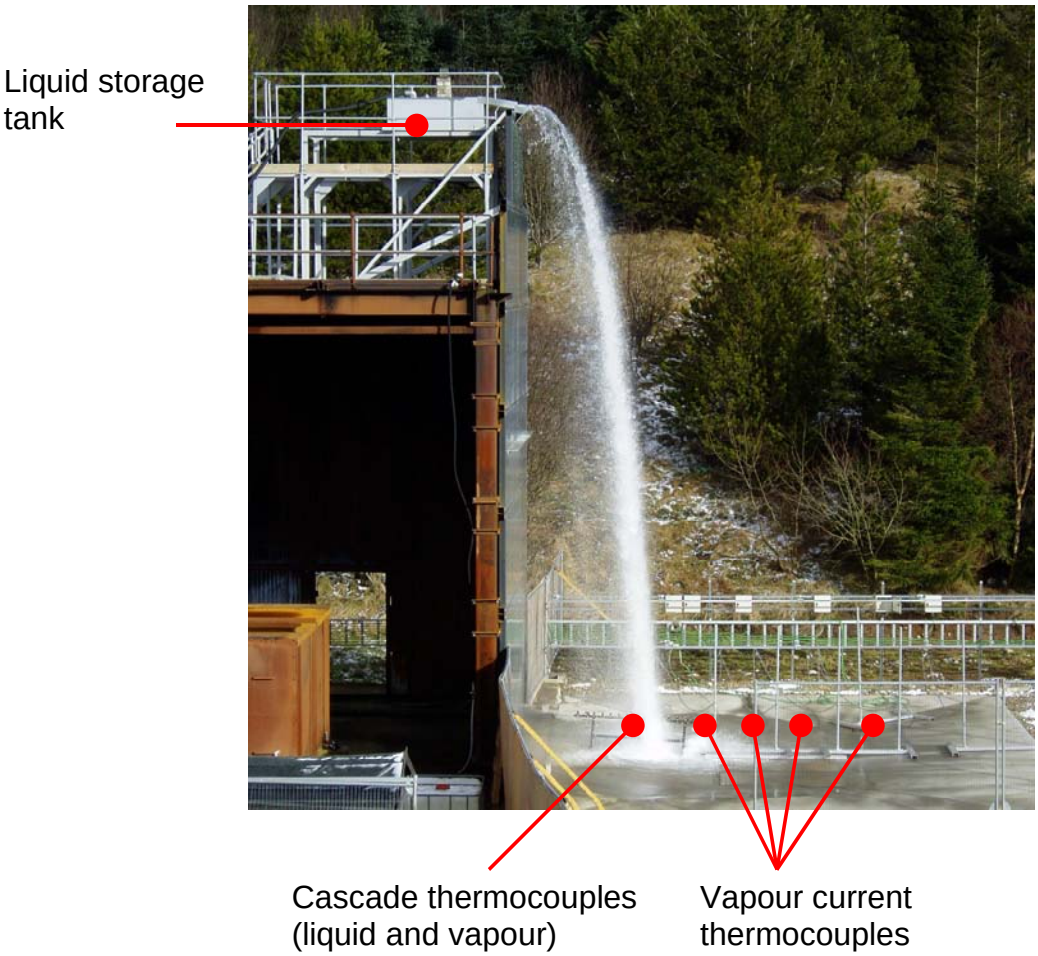

Figure 1 The experimental apparatus showing the measuring locations

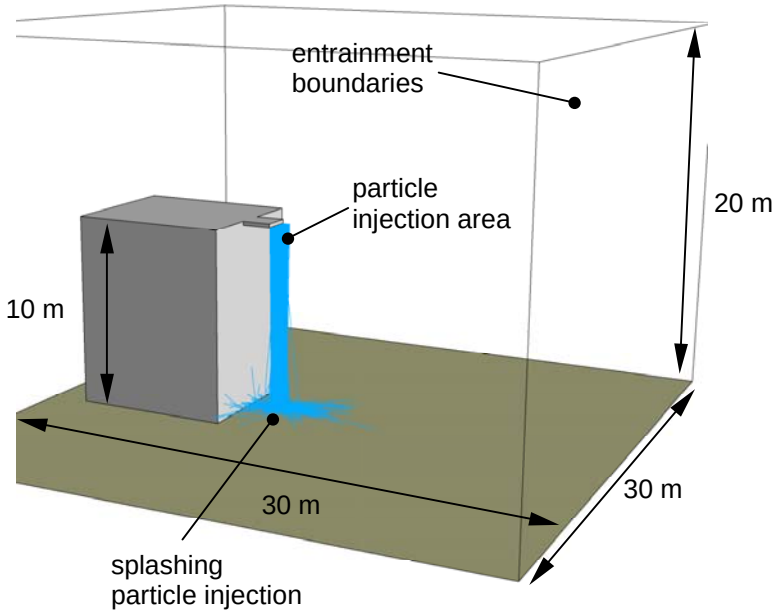

Figure 2 Computational geometry

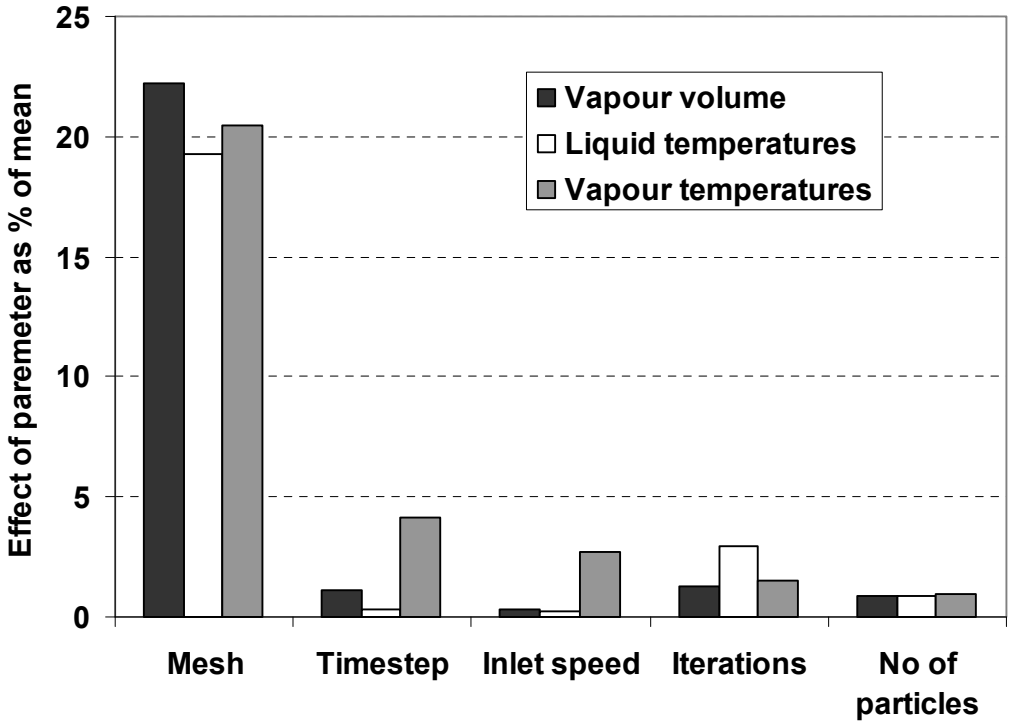

Figure 3 Relative sensitivity to numerical inputs

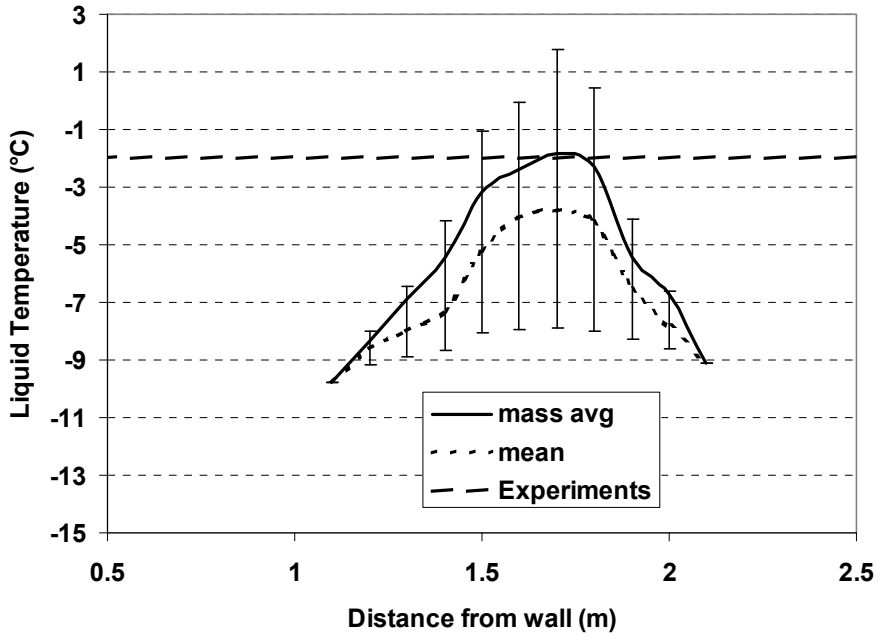

Figure 4 Averaged droplet temperatures across the depth of the cascade

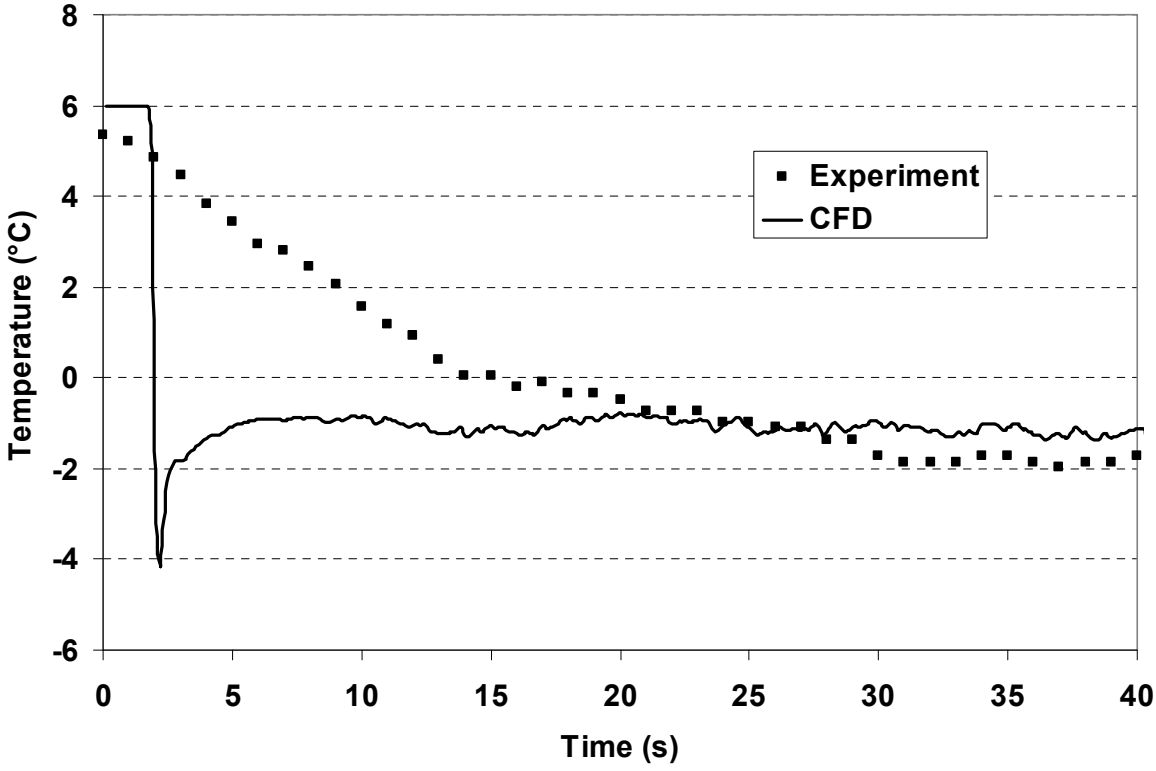

Figure 5 Vapour temperatures at the centre of the cascade

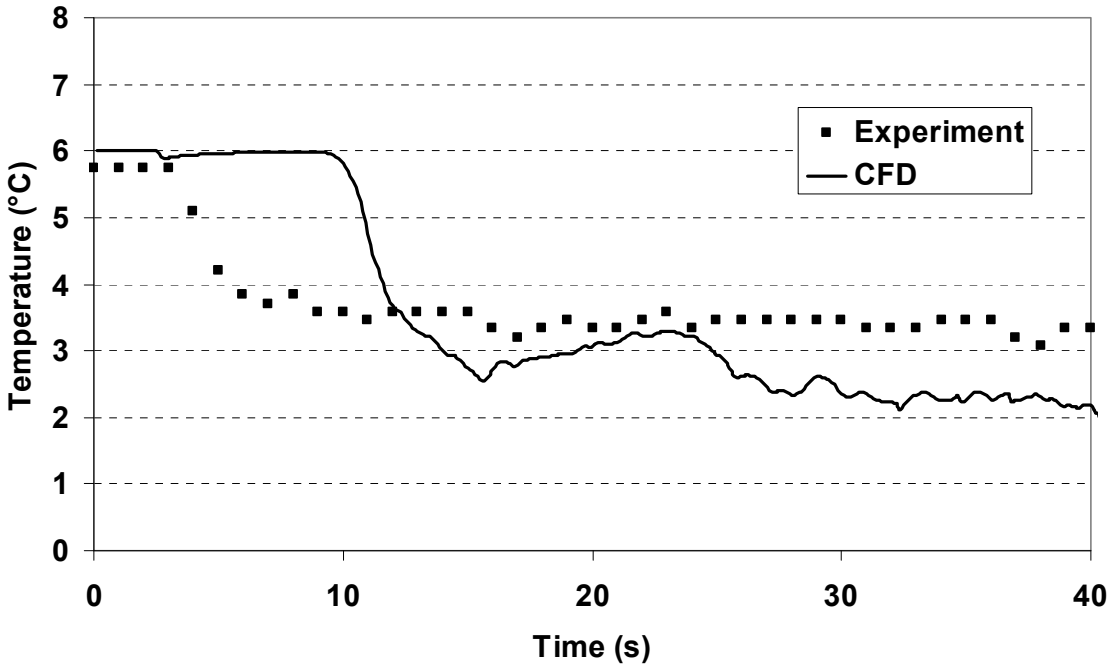

Figure 6 Vapour temperatures 5 m from the wall and 0.5 m from the ground

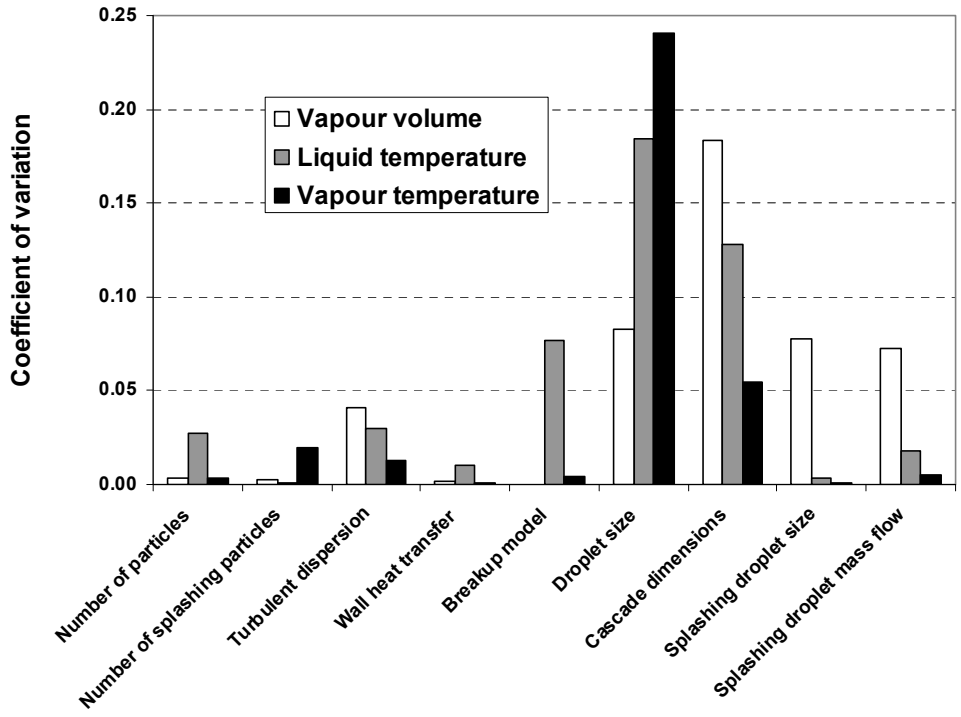

Figure 7 Sensitivity of the model to inputs

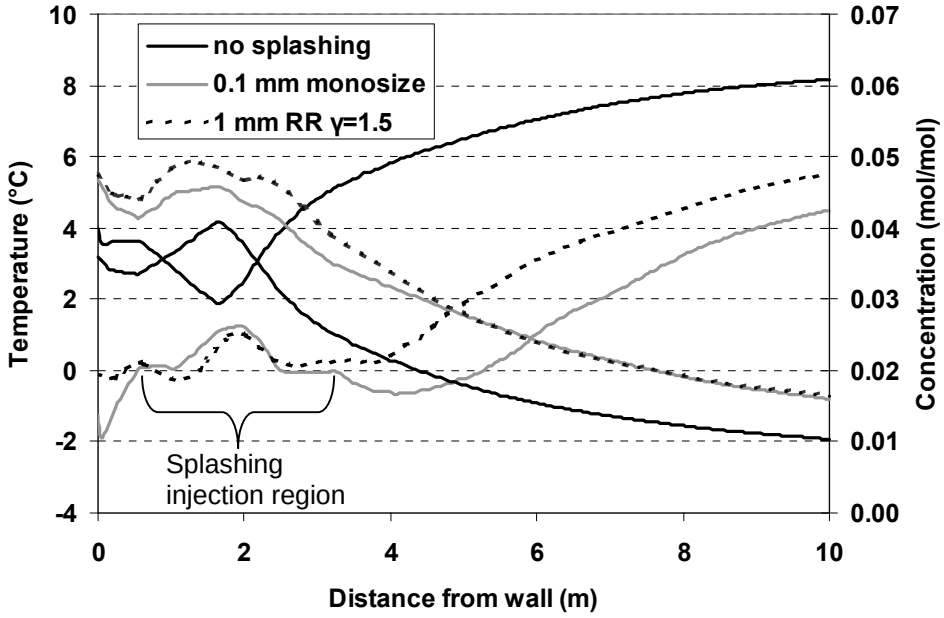

Figure 8 Concentration and temperature on a line extending from the tank wall at a height of 0.15 m from the ground (concentrations showing a downward trend)

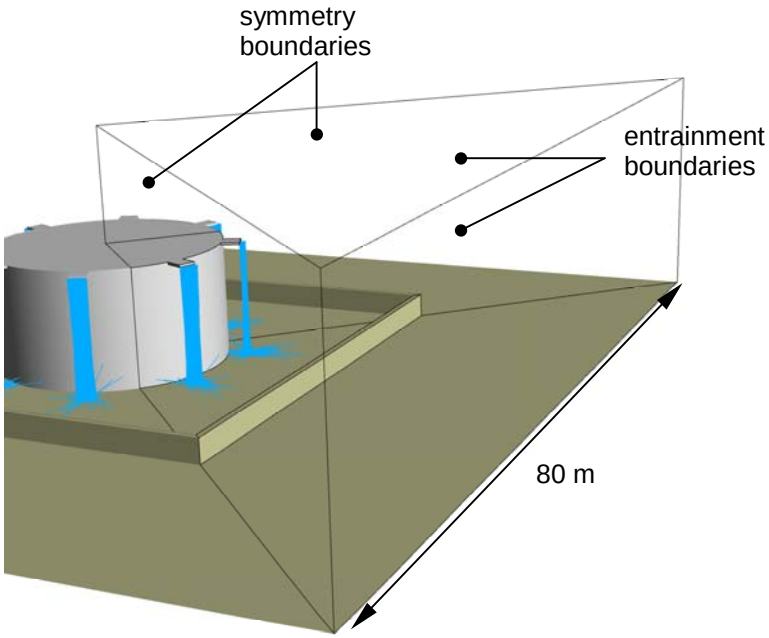

Figure 9 Computational geometry for Cases C to H. The triangular section identified by the wireframe was modelled.

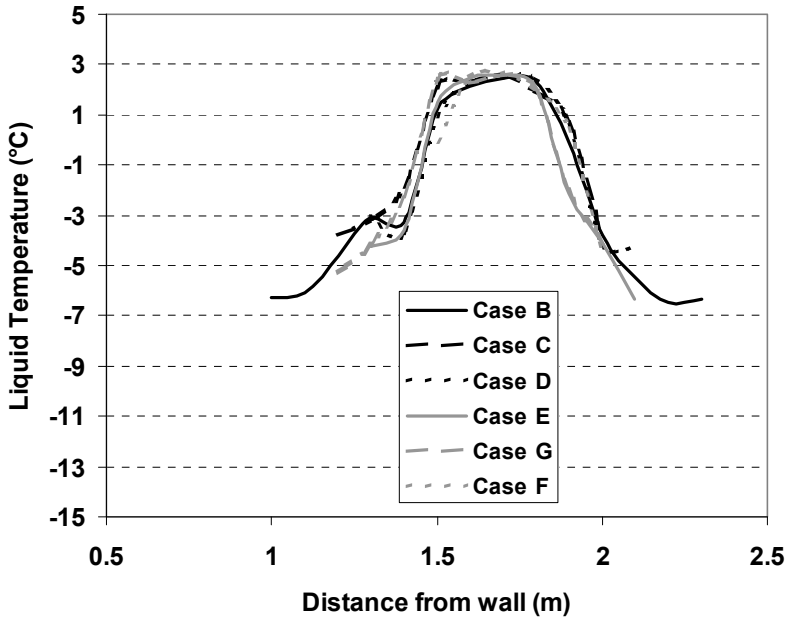

Figure 10 Liquid temperatures for the initial 10-60 second period of each simulation

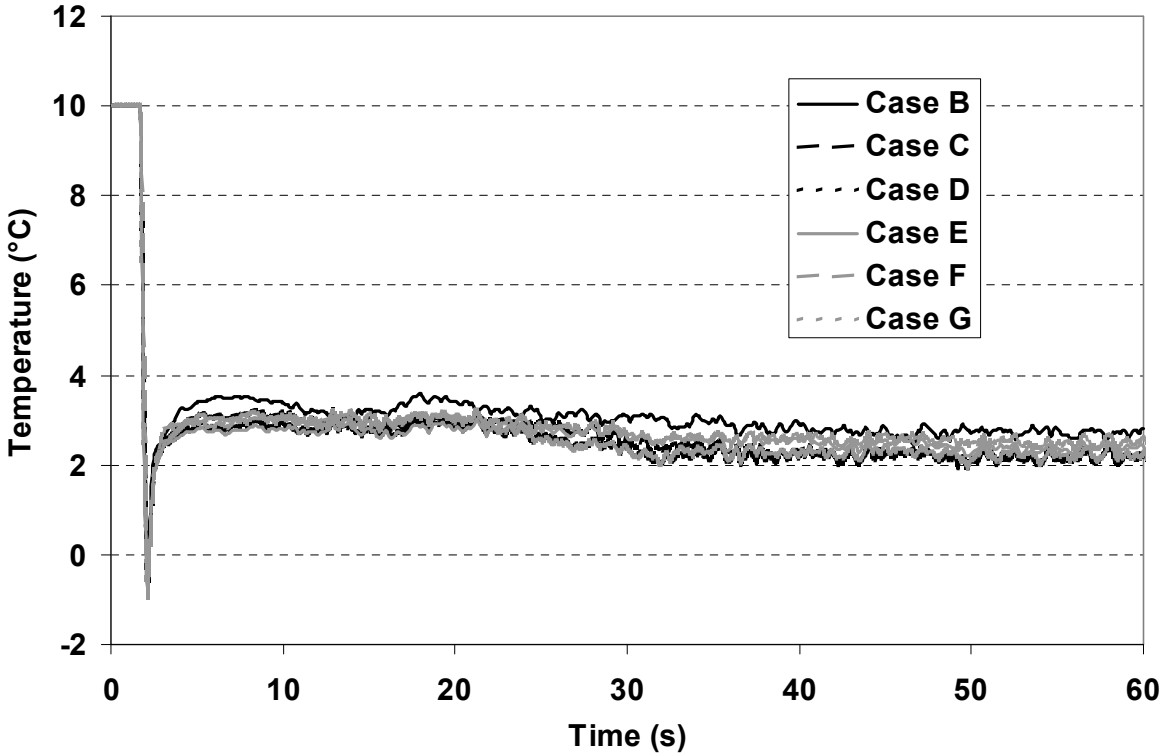

Figure 11 Vapour temperatures at the centre of the cascade

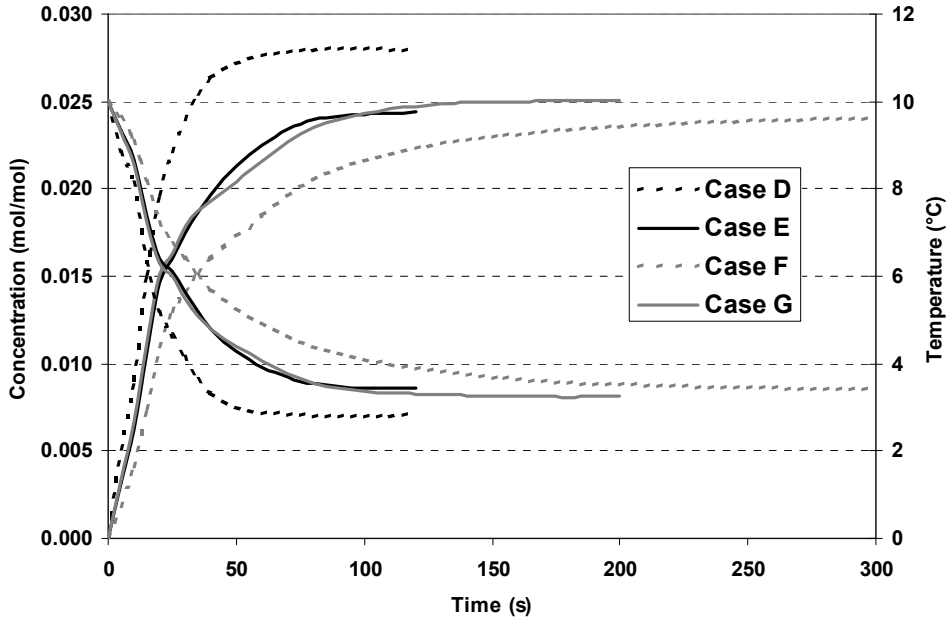

Figure 12 Average vapour concentration and temperature within the bund (ambient temperature is 10ºC)

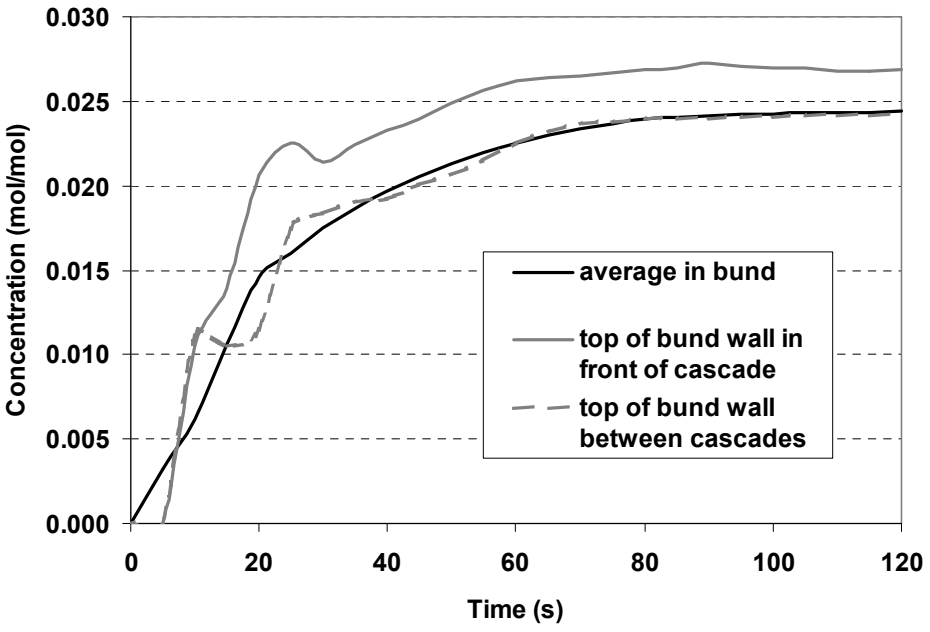

Figure 13 Average vapour concentration in the bund and average vapour concentration flowing over the bund wall (Case E)

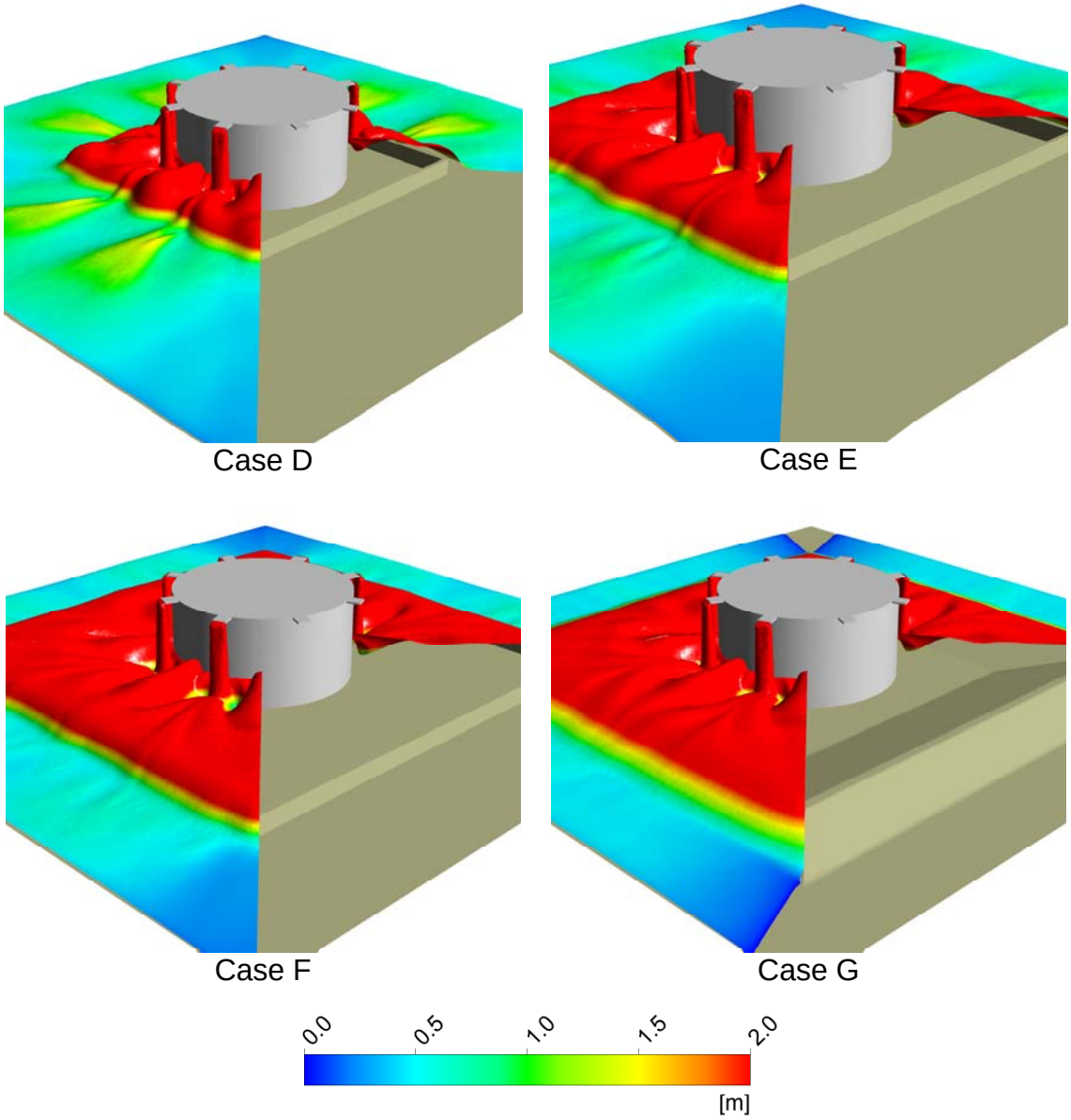

Figure 14 Isosurfaces of vapour concentration at the LFL. The surfaces are coloured according to height from the ground, up to a maximum of two metres

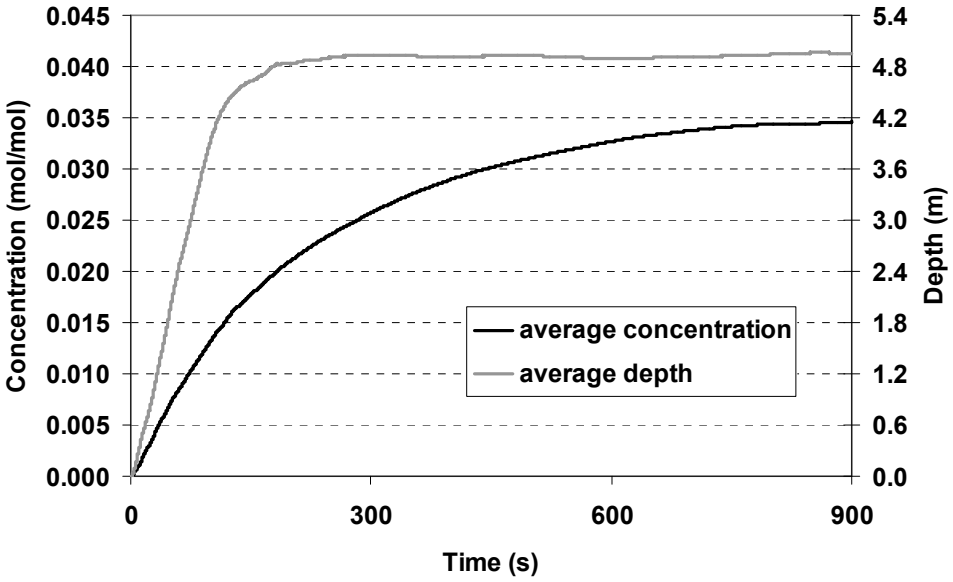

Figure 15 Average concentration of the accumulating layer and depth to ½ LFL

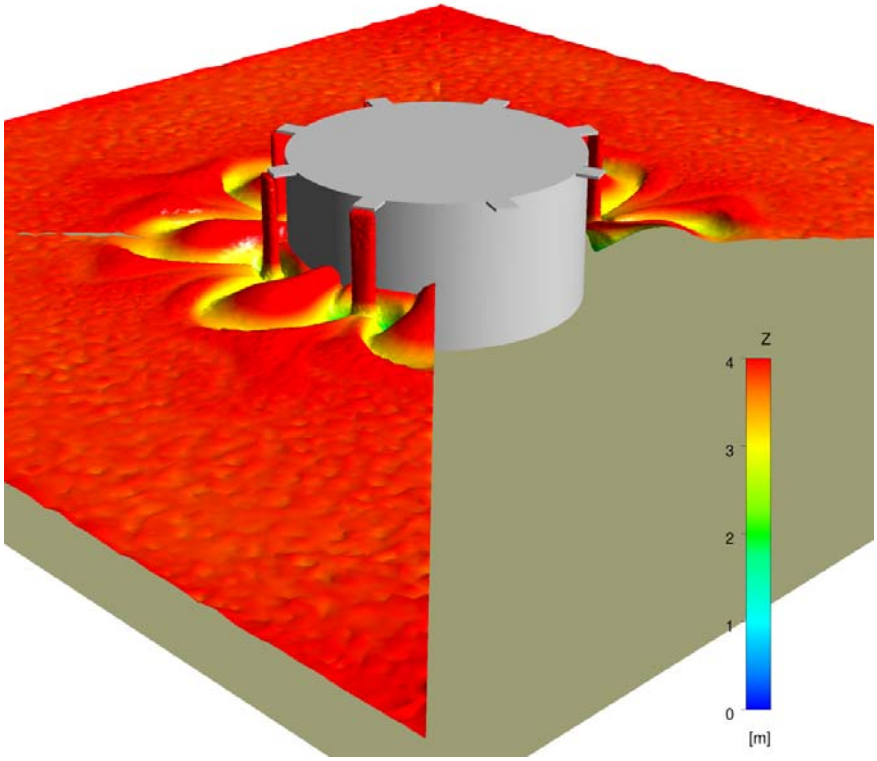

Figure 16 Isosurface at twice the LFL after 10 minutes. The surface is coloured according to height from the ground, up to a maximum of four metres

Table 1 High and low values of the chosen simulation parameters

Parameter	***Low value***	***High value***
Mesh nodes (1000's)	148	60
Timestep (s)	0.05	0.1
Particle inlet speed (m/s)	0.5	1
Number of iterations	5	9
Number of particles	500	1000

Table 2 Arrangement of simulations for the fractional factorial experiment

Run	***Mesh nodes (1000's)***	***Timestep(s)***	***Inlet speed (m/s)***	***Iterations***	***No. of particles***
1	148	0.05	0.5	5	1000
2	148	0.05	1	9	500
3	148	0.1	0.5	9	500
4	148	0.1	1	5	1000
5	60	0.05	0.5	9	1000
6	60	0.05	1	5	500
7	60	0.1	0.5	5	500
8	60	0.1	1	9	1000

Table 3 Other computational inputs for the fractional factorial design

Parameter	***Setting***
Hexane flowrate (kg/s)	11.8
Air temperature (°C)	6
Liquid temperature (°C)	6.4
Turbulence model	SST
Turbulence intensity (%)	5
Eddy viscosity ratio	10

Table 4 Computational settings for the two best fit simulations

Parameter	***Case A***	***Case B***
Test	9	12
Air temperature (°C)	6	10
Liquid starting temperature (°C)	6.4	12.6
Mass flow (kg/s)	11.8	15
Particle size in cascade	2 mm, $\gamma = 3$	2 mm $\gamma = 3$
Splashing particle mass flow (% of liquid flow)	10	10
Splashing particle size	0.1 mm	0.1 mm
Splashing particle velocity (m/s)	3	3
Splashing particle temperature (°C)	-3.4	0.33

Table 5 Configurations for the circular tank simulations

Simulation	***Configuration***	
Case C	no bund	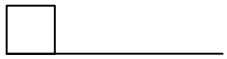
Case D	bund at 5 m	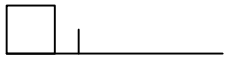
Case E	bund at 10 m	
Case F	bund at 15 m	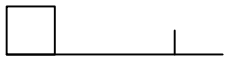
Case G	sloping bund at 5 m	
Case H	no bund, 4m wall surrounding domain	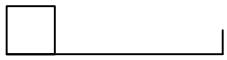

Table 6 Cascade vapour and liquid temperature between the start and end of the simulations

	Temperature difference (start-end) (°C)	
	Vapour	***Liquid***
Case C	0.3	0.5
Case D	0.2	0.9
Case E	0.3	0.4
Case F	0.3	0.1